Electric Power Systems Research 89 (2012) 129–138

Contents lists available at SciVerse ScienceDirect

Electric Power Systems Research

journal homepage: www.elsevier.com/locate/epsr

Probabilistic load flow for photovoltaic distributed generation using the Cornish–Fisher expansion

F.J. Ruiz-Rodriguez [a], J.C. Hernández [b], F. Jurado [a,*]

[a] Department of Electrical Engineering, University of Jaén, 23700 EPS Linares, Jaén, Spain
[b] Department of Electrical Engineering, University of Jaén, 23071 EPS Jaén, Spain

ARTICLE INFO

Article history:
Received 12 March 2011
Received in revised form 6 February 2012
Accepted 12 March 2012
Available online 6 April 2012

Keywords:
Irradiance
Probability density function
Distributed generation
Monte Carlo method
Probabilistic load flow

ABSTRACT

This paper shows that in order to solve a probabilistic load flow in radial distribution networks, it is necessary to apply effective techniques that take into account their technical constraints. Among these constraints, voltage regulation is one of the principal problems to be addressed in photovoltaic distributed generation. Probabilistic load flows can be solved by analytical techniques as well as the Monte Carlo method. Our research study applied an analytical method that combined the cumulant method with the Cornish–Fisher expansion to solve this problem. The Monte Carlo method is used to compare the results of analytical method proposed.

To evaluate the performance of photovoltaic distributed generation, this paper describes a probabilistic model that takes into account the random nature of solar irradiance. Therefore, load and photovoltaic distributed generation are modelled as independent/dependent random variables.

The results obtained show that the technique proposed gave a better performance than the Monte Carlo method. This technique provided satisfactory solutions with a smaller number of iterations. Therefore, convergence was rapidly attained and computational cost was lower than that required for the Monte Carlo method. Besides, the results revealed how the Cornish–Fisher expansion had a better performance than the Gram–Charlier expansion, when input random variables were non-Gaussian.

© 2012 Elsevier B.V. All rights reserved.

1. Introduction

Until now, the main function of distribution networks has been limited to connecting central generation and transmission networks to the end consumers. As a result, distribution networks have always been regarded as passive networks. However, the wide use of DG is in the process of transforming them and making them more active [1].

DG can affect voltage profiles since when a generator operates in a network, this causes the voltage to increase. Although, this has the advantage of making the security margin greater and of reducing losses, it can also lead to overvoltages, especially in the neighbourhood of the DG unit [2].

The connection rules and criteria for the penetration of DG are based on a deterministic steady state analysis. However, deterministic load flow analysis cannot objectively measure how often or specify the location where overvoltages or undervoltages will occur in the network over a given time period. This can be accomplished by using the probabilistic load flow based on analytical techniques or the Monte Carlo method [3]. Probabilistic load flow is described in [4,5], and is further developed in [6,7]. A new simulation method for a composite power system is proposed in [8] in order to evaluate the probability distribution function of branch flows and node voltage magnitudes.

Ref. [9] describes a study of probabilistic load flow using the cumulant method combined with the Gram–Charlier expansion to characterise the output random variables of the problem. The cumulant method exploits the properties of the convolution of random variables [10]. Another analytical technique for characterising these variables is one that combines the cumulant method with Von Mises functions [11]. Although this technique gives a better approximation than the Gram–Charlier expansion, it comes with a higher computational cost.

Despite the fact that they are somewhat less accurate, the advantage of analytical techniques, as opposed to the Monte Carlo method, is their lower computational cost.

Probabilistic techniques can also be effectively applied to analyse the optimal power flow of the systems [12,13]. The point estimate method is used in [14,15] to solve the probabilistic load flow. In Refs. [16–18], the probabilistic load flow is used in meshed power systems with wind generation.

To evaluate the performance of PV generators in large radial distribution networks, this paper proposes an analytical technique

* Corresponding author. Tel.: +34 953 648518; fax: +34 953 648586.
E-mail addresses: fjruiz@ujaen.es (F.J. Ruiz-Rodriguez), jcasa@ujaen.es (J.C. Hernández), fjurado@ujaen.es (F. Jurado).

0378-7796/$ – see front matter © 2012 Elsevier B.V. All rights reserved.
doi:10.1016/j.epsr.2012.03.009

for probabilistic load flow based on the cumulant method combined with the Cornish–Fisher expansion. Probabilistic load flow has typically included the uncertainty of load, which is modelled with Gaussian PDFs. However, the PV energy growth poses new challenges, since the variability of PV power production is much higher, and the PDF of the uncertainties is not Gaussian [19,20]. Moreover, the uncertainties of PV power injections in geographically close PV generators are dependent on each other. As PV PDF has not as yet been satisfactorily modelled, this paper proposes a probabilistic PV model to be included in the probabilistic radial load flow. The technique proposed is an improvement over the previous approach in [21,22] because there is a substantial enhancement in the modelling of PV power production and loads. Although the time interval considered in this technique is 1 h, shorter intervals of time can be considered by varying the correlation of PV dependence and the distribution functions of load and PV power injection.

In general, the technique proposed in this paper combines different approaches. However, it is based on the cumulant method, generalised for the case of dependent random variables. Additionally, a more refined method [23] to solve the load flow in radial distribution systems is applied because the traditional Newton–Raphson method produces convergence problems in these systems.

2. Probabilistic PV system model

Solar irradiation on a horizontal surface inside the atmosphere cannot be accurately predicted since it depends on the irregular presence of clouds. The randomness produced by clouds on terrestrial irradiation is characterised by two random variables [24,25]: the daily clearness index K_T and the hourly diffuse fraction k_d.

The characterisation of the behaviour of global irradiation [24,26–30] and of diffuse irradiation [25,27,31–33] makes it possible to construct a probability model (using PDFs and CDFs) for indexes, K_T [24,27–29] and k_d [25]. Thus, the statistical properties of global irradiation are first described in terms of the daily clearness index [24,27–30]:

$$K_T = \frac{H_{g,d}}{H_{0,d}} \tag{1}$$

Hollands and Huget propose the following PDF for the random variable $\boldsymbol{K_T}$ dependent only on $\bar{K}_T$ [24]:

$$p_K(\boldsymbol{K_T}, \bar{K}_T) = C_1 \left(\frac{K_{Tu} - \boldsymbol{K_T}}{K_{Tu}} \right) e^{\lambda_1 \cdot \boldsymbol{K_T}} \tag{2}$$

where C_1 and λ_1 parameters are functions of K_{Tu} and $\bar{K}_T$.

The random variable, daily global irradiation $\boldsymbol{H_{g,d}}$, obtained from Eq. (1) is:

$$\boldsymbol{H_{g,d}} = H_{0,d} \cdot \boldsymbol{K_T} \tag{3}$$

The hourly global irradiation $\boldsymbol{H_{g,h}}$ is obtained from $\boldsymbol{H_{g,d}}$ with the Eq. (4) [34]:

$$r_g = \frac{\boldsymbol{H_{g,h}}}{\boldsymbol{H_{g,d}}} = \frac{H_{0,h}}{H_{0,d}} \cdot \theta(t) \tag{4}$$

Secondly, the statistical properties of diffuse irradiation are described in terms of the hourly diffuse fraction [25,31–33]:

$$k_d = \frac{H_{d,h}}{H_{g,h}} \tag{5}$$

Although most $k_d(k_t)$ available correlations are deterministic, an effective approach [25,31] should consider the fact that this function is not deterministic. In other words, for a given k_t, value, k_d can take a range of values distributed around its mean, $\bar{k}_d$. Using the expected value approach of probability theory, Hollands and Crha

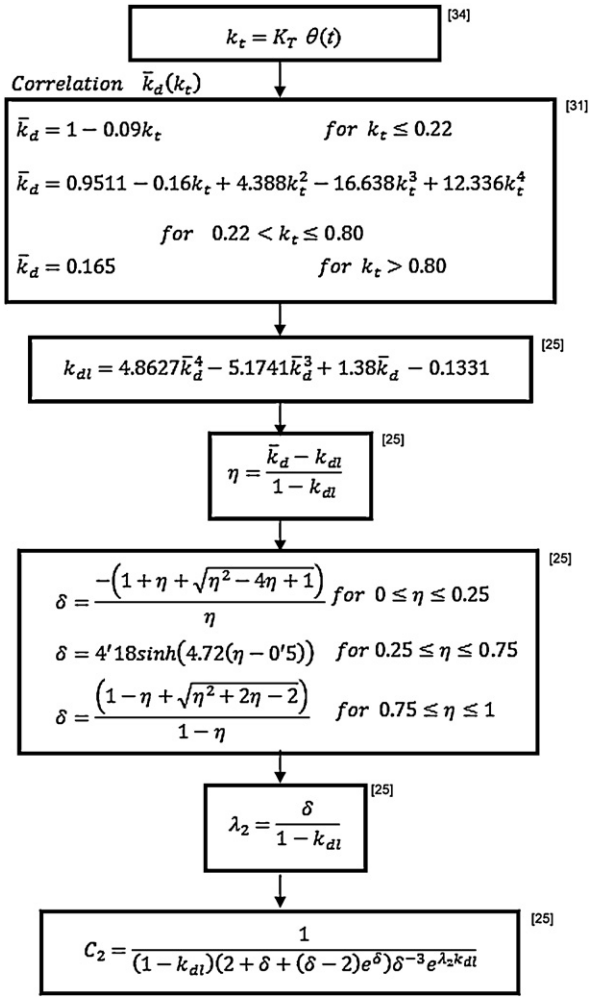

Fig. 1. Flowchart to evaluate C_2, λ_2 and k_{dl} parameters.

[25] gives a general-purpose expression for the PDF of the random variable $\boldsymbol{k_d}$:

$$p_K(\boldsymbol{k_d}, \overline{k_d}) = C_2(\boldsymbol{k_d} - k_{dl}) \cdot (1 - \boldsymbol{k_d}) e^{\lambda_2 \cdot \boldsymbol{k_d}} \tag{6}$$

where C_2, λ_2, and k_{dl} parameters are functions of $\bar{k}_d$, as shown in Fig. 1. The expression for $p_k(\boldsymbol{k_d}, \bar{k}_d)$ is independent of the actual $\bar{k}_d(k_t)$ relation [25,31–33].

The random variable, hourly diffuse irradiation $\boldsymbol{H_{d,h}}$, which combines Eqs. (4) and (5), is given by Eq. (7):

$$\boldsymbol{H_{d,h}} = r_g \cdot H_{g,h} \cdot \boldsymbol{k_d} \tag{7}$$

The hourly global irradiance on a tilted surface G_{g,h_β} can be calculated from the components of the incident irradiance beam ($G_{b,h} = G_{g,h} - G_{d,h}$), diffuse irradiance ($G_{d,h}$), and ground-reflected irradiance ($G_{r,h}$) on the horizontal plane [35]:

$$\begin{aligned} G_{g,h\_\beta} &= (G_{g,h} - G_{d,h}) R_b FT_b(\theta_S) \\ &+ G_{d,h} \left[(1 - \bar{k}_b) \frac{1 + \cos\beta}{2} FT_d(\beta) + R_b \bar{k}_b FT_b(\theta_S) \right] \\ &+ G_{g,h} \rho \left(\frac{1 - \cos\beta}{2} \right) FT_r(\beta) \end{aligned} \tag{8}$$

To determine the diffuse irradiance fraction, the Hay model [36] for anisotropic skies is applied in Eq. (8). Furthermore, the angular losses of each radiation component, $FT_b(\theta_s)$, $FT_d(\beta)$, and $FT_r(\beta)$, follow Ref. [35]. The global, beam, and diffuse irradiance are assumed

to remain constant and equal to the global, beam, and diffuse irradiation, respectively, for the integration period (hourly approach):

$$H_{(g)(b)(d),h}\ (\mathrm{Wh/m^2}) = G_{(g)(b)(d),h}\ (\mathrm{W}/m^2) \cdot 1h \tag{9}$$

This assumption does not generate important errors, and avoids making integrations in the time domain. When the assumption of Eq. (9) is included in Eq. (8), and even though the random variable $\boldsymbol{G_{g,h\_\beta}}$ may depend upon parameters other than the random variables $\boldsymbol{H_{g,h}}$ and $\boldsymbol{H_{d,h}}$ (e.g. β, ρ, FT_b (θ_s), $FT_d(\beta)$, $FT_r(\beta)$, Rb, $\bar{k}_b$), these parameters must be the same for each hour or they may be averaged. Therefore, the hourly global irradiance on a tilted surface is a new random variable, which is a linear combination of the independent random variables, $\boldsymbol{H_{g,h}}$ and $\boldsymbol{H_{d,h}}$:

$$\boldsymbol{G_{g,h\_\beta}} = a_1 \cdot \boldsymbol{H_{g,h}} + a_2 \cdot \boldsymbol{H_{d,h}} \tag{10}$$

where the coefficients a_i in the linear combination are known (functions of β, ρ, $FT_b(\theta_s)$, $FT_d(\beta)$, $FT_{r\_}(\beta)$, R_b and $\bar{k}_b$).

At this point, the cumulant method [37] allows the statistical information mapping of predefined random variables, $\boldsymbol{H_{g,h}}$ and $\boldsymbol{H_{d,h}}$, with the new random variable $\boldsymbol{G_{g,h\_\beta}}$. This information is mapped by means of a statistical measurement known as cumulants. Based on the hourly global irradiance on the plane of the PV array, the random variable, hourly PV electrical power (DC side) $\boldsymbol{P_{pv,h}}$, is calculated in the same way as [35,38]:

$$\boldsymbol{P_{pv,h}} = \xi_c \cdot A \cdot \boldsymbol{G_{g,h\_\beta}} \tag{11}$$

This power depends on the PV cell's electrical efficiency, which has the following familiar linear form [38]:

$$\boldsymbol{\xi_c} = \xi_{ref}\left\{1 - \beta_{ref}\left[T_a - T_{ref} + \frac{\boldsymbol{G_{g,h\_\beta}}}{G_{NOCT}}(T_{NOCT} - T_a)\right]\right\} \tag{12}$$

Assuming in Eq. (12) that the ambient temperature T_a is constant for the hourly period (no random variable), Eq. (11) may be rewritten with coefficients b_1 and b_2 as shown in Eq. (13):

$$\boldsymbol{P_{pv,h}} = (b_1 + b_2 \cdot \boldsymbol{G_{g,h\_\beta}}) \cdot \boldsymbol{G_{g,h\_\beta}} \tag{13}$$

Eq. (13) must be linearised [11] if the cumulant method [37] is used to obtain the statistical information of the new random variable $\boldsymbol{P_{pv,h}}$:

$$\boldsymbol{P_{pv,h}} = b_3 + b_4 \cdot \boldsymbol{G_{g,h\_\beta}} \tag{14}$$

where coefficients b_3 and b_4 are:

$$b_3 = b_1 + 2 \cdot b_2 \cdot \bar{G}_{g,h\_\beta} \tag{15}$$

$$b_4 = -b_2 \cdot \bar{G}^2_{g,h\_\beta} \tag{16}$$

2.1. Random generation of dependent PV power injections

The uncertainty of the PV power prediction of geographically close PV generators is correlated. The reason for this is that the PV power in all of them is due to similar meteorological conditions [39,40]. This dependence has not yet been modelled, but studies such as [41,42] show that there is spatial dependence between production in a wide area. These values can be regarded as an estimate of actual correlation values, but there is still much work to be done.

The method used to generate dependent PV power injections is based on the generation of multivariate dependent random numbers [18]. These numbers are used to numerically obtain the cumulants (moments) and crossed cumulants (moments) required in the analytical technique described in this paper. The numbers are also used for the Monte Carlo simulation process run to check the results of the technique. The way of modelling this dependence is through the correlation matrix of a multivariate normal variable.

The method begins by generating random numbers of a multivariate normal random variable with a given correlation matrix, thus forming the array $\boldsymbol{Y}_1 \in \Re^{n_{rv},m_{rv}}$. Secondly, a multivariate normal transformation is performed of these values in order to obtain a multivariate uniform distribution $\boldsymbol{Y}_2$, where $\boldsymbol{Y}_2 = \Phi(\boldsymbol{Y}_1)$. The third step involves transforming the multivariate uniform random numbers obtained into series with the desired PV marginal distributions $F_{p_{pv,h}}(\boldsymbol{p_{pv,h}})$. Thus, the sample k of the new random variable i, $y_{3,ik}$ is obtained as $y_{3,ik} = F^{-1}_{p_{pv,h}}(y_{2,ik})$. The random numbers with the desired distribution thus have correlations that are very close to the original one of the normal multivariate distribution.

3. Probabilistic load model

The electric load of a power system has deterministic and stochastic components. The two main deterministic factors that affect this load are time (multiple seasonal patterns: yearly, weekly and intra-daily) and weather conditions. However, there is also a random component in the load which cannot be modelled. This component is the result of the random behaviour of energy consumers. Consumers are classified by electric utilities into different subjective classes [43,44].

Typical load patterns of consumer classes can be obtained from the statistical analysis of historical data. Thus, Refs. [43,44] defined TDPs for each consumer class, which contained information about daily load profiles after the extraction of all exogenous information, i.e. seasonal (yearly and weekly cycles) and weather information. Additionally, Jardini et al. [43] applied statistical analysis methods to the TDPs, which allowed them to construct a probability model (using PDFs) capable of giving the probability that a value of a load would be within specified limits. This approach treats the TDPs of each jth consumer class $\boldsymbol{L_j}(m,h)$ as a normally distributed random variable, which changes from month to month and hour to hour. This means that its hourly mean value $\eta_j(m,h)$ and the corresponding standard deviation $\sigma_j(m,h)$ change over the 12-month and 24-h period.

In this study, the Jardini approach was followed to build the TDPs of consumer classes, based on data from a Spanish electrical utility [45]. However, seasonal information when TDPs are elaborated was only partially extracted. Thus, for the jth consumer class two TDPs were specified per month: one for weekends $\boldsymbol{L_j^{we}}(m)$ and another one for working days $\boldsymbol{L_j^{wo}}(m)$. The one-year TDPs were arranged in a two-dimensional layout with 12 columns representing the 12 months of the year and with 2 rows representing weekend or working days.

When the TDPs of consumer classes are known, it is possible to determine the random variable hourly active power consumed by the kth node of a feeder at the mth month and hth hour $\boldsymbol{P_{Lk}}(m,h)$ by adding the random variables $\boldsymbol{L_j}(m,h)$ corresponding to the individual consumption of all consumer classes. For example, for working days:

$$\boldsymbol{P^{wo}_{Lk}}(m,h) = \sum_{j=1}^{n_{cc}} cn_{j,k} \cdot \boldsymbol{L^{wo}_j}(m,h) \tag{17}$$

Assuming a deterministic power factor, the relevant reactive power consumed is the following:

$$\boldsymbol{Q_{Lk}}(m,h) = \boldsymbol{P_{Lk}}(m,h) \cdot \tan\varphi \tag{18}$$

4. Probabilistic radial load flow

The method used in this study to solve deterministic load flow for radial distribution systems is described in [23]. The Newton–Raphson method does not satisfactorily solve the classical load flow in radial distribution systems because it gives convergence problems.

The classical load flow is given by a system of nonlinear equations that represents it. They represent the steady-state balance in the network between the power consumed and power produced:

$$P_i = V_i \sum_{k=1}^{N_n} [V_k (G_{ik} \cos \delta_{ik} + B_{ik} \operatorname{sen} \delta_{ik})]$$
$$Q_i = V_i \sum_{k=1}^{N_n} [V_k (G_{ik} \operatorname{sen} \delta_{ik} - B_{ik} \cos \delta_{ik})] \quad (19)$$

These input values to the problem cannot be accurately determined in a probabilistic approach. However, one way to better characterise the sources of uncertainty of the system is to represent the input data as random variables in the problem. In this respect, the Monte Carlo method [3] is an important simulation technique that makes it possible to continue using the deterministic load flow algorithms. There are also analytical ways of dealing with the problem of probabilistic load flow [11]. Such techniques use the properties of the convolution of random variables.

4.1. Monte Carlo method

This method is the most straightforward method of solving the probabilistic power flow. It is basically used to randomly select values of input variables from their distribution functions, and with these values, solve a deterministic radial load flow, as explained in [23]. After a certain number of simulations, the probabilistic solution of the problem is reconstructed from deterministic data obtained for each simulation.

It should be underlined that the number of simulations needed to obtain an accurate result with the Monte Carlo method is independent of system size [10]. For an accurate representation, many simulations must be considered (approximately 10,000 [8,46]), which sometimes makes this approach impractical. Since the computation time of the Monte Carlo method is longer as the number of simulations increases, it is important to determine the accuracy of the results. This can be quantified by means of the relative error of the Monte Carlo method for a given number of simulations n [9,10]:

$$\varepsilon_{MC} = \frac{100}{(n_T - 1) \cdot N_n} \sum_{i=1}^{N_n} \sum_{j=2}^{n_T} \frac{|\bar{V}_i^{j-1} - \bar{V}_i^j|}{\bar{V}_i^j} \quad (20)$$

where $\bar{V}_i^j$ is the mean voltage at node ith for the test group jth (e.g. second test of a total test number n_T equal to 50), given a number of simulations n (e.g. 10,000 simulations). Thus, in Eq. (20), the Monte Carlo method is used to execute a given number of simulations n (e.g. 10,000 simulations) several times n_T (e.g. 50 times). The solutions obtained are compared in such a way that for two different test groups of the same number of simulations n (e.g. first test group of 10,000 simulations and second test group of 10,000 simulations), the error between both groups is relatively small. It can be observed that for a certain n, even though the number of simulations increases, the average values and standard deviation obtained do not sensibly change, and the difference between the solutions of the groups is very small [9].

In the Monte Carlo method, the mean of a random variable $\boldsymbol{x}$ is determined by the following equation:

$$\bar{x} = \eta_{\boldsymbol{x}} = \sum_{i=1}^{n} \frac{x_i}{n} \quad (21)$$

The standard deviation of a random variable $\boldsymbol{x}$ is determined by the equation:

$$\sigma_x = \sqrt{\frac{\sum_{i=1}^{n} (x_i - \bar{x})^2}{(n-1)}} \quad (22)$$

4.2. Analytical technique

4.2.1. Linear approximation

The linearisation process of load flow equations (Eq. (19)) is performed around the solution obtained with a deterministic load flow, based particularly on the expected values of the system. These expected values are obtained after solving the problem of the deterministic radial load flow [23]. To illustrate this technique, two random variables $\boldsymbol{x}$ and $\boldsymbol{y}$ are considered. At some point in the problem, these random variables are multiplied to give a third random variable $\boldsymbol{z}$:

$$z = \boldsymbol{x} \cdot \boldsymbol{y} \quad (23)$$

If the deviations of $\boldsymbol{x}$ and $\boldsymbol{y}$ are represented around their mean values $\eta_{\boldsymbol{x}}$ and $\eta_{\boldsymbol{y}}$ by $\Delta\boldsymbol{x}$ and $\Delta\boldsymbol{y}$ respectively, the following can be assumed:

$$\boldsymbol{x} = \eta_{\boldsymbol{x}} + \Delta\boldsymbol{x} \quad \boldsymbol{y} = \eta_{\boldsymbol{y}} + \Delta\boldsymbol{y} \quad (24)$$

When second-order terms are not considered, Eq. (25) is obtained:

$$z \approx \eta_{\boldsymbol{x}} \cdot \eta_{\boldsymbol{y}} + \eta_{\boldsymbol{x}} \cdot \Delta\boldsymbol{y} + \eta_{\boldsymbol{y}} \cdot \Delta\boldsymbol{x} = \eta_{\boldsymbol{x}} \cdot y + \eta_{\boldsymbol{y}} \cdot x - \eta_{\boldsymbol{x}} \cdot \eta_{\boldsymbol{y}} \quad (25)$$

Therefore, if changes of random variables are small, the variable $\boldsymbol{z}$ can be linearised since the expected values $\boldsymbol{x}$ and $\boldsymbol{y}$ are known. This technique can be applied to the angles and voltages in the load flow equations (Eq. (19)). Thus, the following results are obtained:

$$P_i = \sum_{k=1}^{N_n} [e'_{ik} + f'_{ik} \cdot \delta_i - f'_{ik} \cdot \delta_k + g'_{ik} \cdot V_i + h'_{ik} \cdot V_k]$$
$$Q_i = \sum_{k=1}^{N_n} [e''_{ik} + f''_{ik} \cdot \delta_i - f''_{ik} \cdot \delta_k + g''_{ik} \cdot V_i + h''_{ik} \cdot V_k] \quad (26)$$

where the coefficients $e', f', g', h', e'', f'', g''$, and h'' are calculated from system parameters and expected values for the variables [10].

4.2.2. Moments and cumulants

The moments of a random variable $\boldsymbol{x}$ are the expected values of certain functions of $\boldsymbol{x}$ [18,47,48]. These are a collection of descriptive measurements that can be used to characterise the probability distribution of $\boldsymbol{x}$ and to determine it if all the moments of $\boldsymbol{x}$ are known. For example, for the case of a multivariate random variable, $\boldsymbol{X} = (\boldsymbol{x}_1, \ldots, \boldsymbol{x}_n)$ with a joint probability density function $f_{\boldsymbol{X}}(\boldsymbol{X})$, the third order moments are defined as [18]:

$$m_{\boldsymbol{X}}^{ijk} = E[x_i x_j x_k] = \iint \int_{-\infty}^{\infty} x_i x_j x_k f_{\boldsymbol{X}}(\boldsymbol{X})\, d\boldsymbol{X} \quad (27)$$

Other moments are defined in a similar way. For instance, third-order central moments can be expressed as:

$$\mu_{\boldsymbol{X}}^{ijk} = E[(x_i - m_{\boldsymbol{X}}^i)(x_j - m_{\boldsymbol{X}}^j)(x_k - m_{\boldsymbol{X}}^k)]$$
$$= \iint \int_{-\infty}^{\infty} (x_i - m_{\boldsymbol{X}}^i)(x_j - m_{\boldsymbol{X}}^j)(x_k - m_{\boldsymbol{X}}^k) f_{\boldsymbol{X}}(\boldsymbol{X})\, d\boldsymbol{X} \quad (28)$$

The cumulants of a random variable are a number of constants that reveal the properties of $\boldsymbol{x}$ and determine its distribution function [48]. Despite the fact that moments and cumulants are related [18,49], cumulants have a number of properties that make their

manipulation even more useful when they are applied to a linear combination of random variables [49]. Thus, let $\boldsymbol{z}$ be a random variable that is a linear combination of a multivariate random variable, $\boldsymbol{X} = (\boldsymbol{x}_1, \ldots, \boldsymbol{x}_{n_{rv}})$, given by:

$$z = \sum_{i=1}^{n_{rv}} a_i \cdot \boldsymbol{x}_i \tag{29}$$

where a_i is real constants.

For example, the third-order cumulant of the random variable $\boldsymbol{z}$ can be expressed as a function of the cumulants of the multivariate random variable $\boldsymbol{X}$ as:

$$k_z^{111} = \sum_{i=1}^{n_{rv}} \cdot \sum_{j=1}^{n_{rv}} \cdot \sum_{k=1}^{n_{rv}} a_i \cdot a_j \cdot a_k \cdot k_{\boldsymbol{X}}^{ijk} \tag{30}$$

In general, the cumulants of order r can be obtained as:

$$k_z^{\overbrace{1\ldots1}^{r}} = \sum_{i_1=1}^{n_{rv}} \overbrace{\cdots}^{r} \sum_{i_r=1}^{n_{rv}} a_{i_1} \overbrace{\cdots}^{r} a_{i_r} \cdot k_{\boldsymbol{X}}^{i_1 \ldots i_r} \tag{31}$$

In general, it is better to use cumulants instead of moments because [49]:

- For independent random variables, the cumulants of a sum are the sums of cumulants.
- For independent random variables, the cross cumulants are zero, while not all the crossed moments are zero.
- Cornish–Fisher expansion is better indicated using cumulants.

4.2.3. Resolution technique of the probabilistic radial load flow

The technique used to solve the probabilistic radial load flow with the method proposed involves obtaining the cumulants of the solution by solving the system of equations of the problem for each order of the cumulants of the input variables [9]. Thus, the cumulant method is used to replace the convolution of the dependent/independent random variables by the linear combination of their cumulants [49]. For independent variables, the crossed cumulants are zero. Cumulants and crossed cumulants of dependent variables can be easily obtained in [18]. The cumulant method allows the use of any random variables and not just normal distributions. This technique reduces the computational burden which is one of the disadvantages of the Monte Carlo method [9,50].

When the cumulants of the distributions of output variables are known, it is possible to reconstruct their CDFs by using the Gram–Charlier or Cornish–Fisher expansion.

In order to obtain the moments (cumulants) and crossed moments (cumulants) of input-dependent PV variables, a set of scenarios is first obtained by generating correlated random numbers as shown in Section 2.1 for the given PDF of the uncertainty. The moments are then numerically obtained by the discretisation of Eq. (27), or its equivalent for moments of a different order. Cumulants and crossed cumulants are obtained from these values by using the equations in [49].

4.2.4. Gram–Charlier expansion

The Gram–Charlier expansion is a way to characterise the resulting random variables of the probabilistic load flow [9,51]. On the basis of the central moments of a given distribution, this technique provides an approximation based on the normal distribution. In practice, it extends to the seventh element of this expansion [48], but its accuracy depends on the number of cumulants [21,22].

Let $\boldsymbol{\varsigma}$ be a random variable with mean $\eta_{\boldsymbol{\gamma}}$ and standard deviation $\sigma_{\boldsymbol{\gamma}}$. According to the Gram–Charlier expansion, the cumulative distribution function $F_{\boldsymbol{x}}(\boldsymbol{x})$ and the probability density function $f_{\boldsymbol{x}}(\boldsymbol{x})$ of the normalised variable $\boldsymbol{x} = \boldsymbol{\varsigma} - \eta_{\boldsymbol{\gamma}}/\sigma_{\boldsymbol{\gamma}}$ can be expressed as a series composed of a standard normal distribution and their derivatives:

$$F_{\boldsymbol{x}}(\boldsymbol{x}) = \Phi(\boldsymbol{x}) + \frac{c_1}{1!}\Phi'(\boldsymbol{x}) + \frac{c_2}{2!}\Phi'''(\boldsymbol{x}) + \frac{c_2}{3!}\Phi'''(\boldsymbol{x}) + \cdots \tag{32}$$

$$f_{\boldsymbol{x}}(\boldsymbol{x}) = \phi(\boldsymbol{x}) + \frac{c_1}{1!}\phi'(\boldsymbol{x}) + \frac{c_2}{2!}\phi''(\boldsymbol{x}) + \frac{c_2}{3!}\phi'''(\boldsymbol{x}) + \cdots \tag{33}$$

where $\Phi(\boldsymbol{x})$ and $\phi(\boldsymbol{x})$ are CDF and PDF, respectively, of a normal $N(0,1)$ distribution ($\eta_{\boldsymbol{x}} = 0$, $\sigma_{\boldsymbol{x}} = 1$), and $\Phi'(\boldsymbol{x})$, $\phi'(\boldsymbol{x})$, $\Phi''(\boldsymbol{x})$, $\phi''(\boldsymbol{x})$... their successive derivatives.

The coefficients c_k are constants that are defined by Eq. (34):

$$c_k = (-1)^k \int_{-\infty}^{\infty} H_k(\boldsymbol{x}) \cdot f_{\boldsymbol{x}}(\boldsymbol{x})\, d\boldsymbol{x} \quad k = 1,\ 2,\ 3, \ldots \tag{34}$$

4.2.5. Cornish–Fisher expansion

The Cornish–Fisher expansion is a formula for approximating the q-quantile of a cumulative distribution function $F_X(\boldsymbol{x})$ in terms of the quantile of a normal $N(0,1)$ distribution $\Phi(\boldsymbol{x})$ and the cumulants of the $F_X(\boldsymbol{x})$. The cumulants of a random variable are conceptually similar to its moments. Suppose a random variable $\boldsymbol{x}$ has a mean of 0 and standard deviation of 1. Cornish and Fisher [51] provide an expansion for approximating the q-quantile, $\Phi_x^{-1}(q)$, of $\boldsymbol{x}$, based upon its cumulants k_x^r and the q-quantile of a standard normal random variable $\Phi^{-1}(q)$. For example, the Cornish–Fisher expansion using the first five cumulants, is shown in Eq. (35) [16–18]:

$$\begin{aligned}\Phi_{\boldsymbol{x}}^{-1}(q) \approx{}& \Phi^{-1}(q) + \frac{\Phi^{-1}(q)^2 - 1}{6}k_{\boldsymbol{x}}^3 + \frac{\Phi^{-1}(q)^3 - 3\Phi^{-1}(q)}{24}k_{\boldsymbol{x}}^4 \\ &- \frac{2\Phi^{-1}(q)^3 - 5\Phi^{-1}(q)}{36}(k_{\boldsymbol{x}}^3)^2 + \frac{\Phi^{-1}(q)^4 - 6\Phi^{-1}(q)^2 + 3}{120}k_{\boldsymbol{x}}^5 \\ &- \frac{\Phi^{-1}(q)^4 - 5\Phi^{-1}(q)^2 + 2}{24}k_{\boldsymbol{x}}^3 \cdot k_{\boldsymbol{x}}^4 \\ &+ \frac{12\Phi^{-1}(q)^4 - 53\Phi^{-1}(q)^2 + 17}{324}(k_{\boldsymbol{x}}^3)^3\end{aligned} \tag{35}$$

Although this equation applies only if $\boldsymbol{x}$ has mean of 0 and standard deviation of 1, it can still be used to approximate the q-quantile if $\boldsymbol{x}$ has some other mean $\eta_{\boldsymbol{x}}$ and standard deviation $\sigma_{\boldsymbol{x}}$. The normalisation of $\boldsymbol{x}$ can be simply defined as shown in Eq. (36):

$$\boldsymbol{x}^* = \frac{\boldsymbol{x} - \eta_{\boldsymbol{x}}}{\sigma_{\boldsymbol{x}}} \tag{36}$$

which has a mean of 0 and a standard deviation of 1. Central moments of $\boldsymbol{x}^*$ can be calculated from central moments of $\boldsymbol{x}$ with:

$$\mu_{\boldsymbol{x}^*}^r = \frac{\mu_{\boldsymbol{x}}^r}{\sigma_{\boldsymbol{x}}^r} \tag{37}$$

When the Cornish–Fisher expansion is applied to obtain the q-quantile $\boldsymbol{x}^*$ of $\boldsymbol{x}^*$, the corresponding q-quantile x of $\boldsymbol{x}$ is as shown in Eq. (38):

$$\boldsymbol{x} = \boldsymbol{x}^* \cdot \sigma_{\boldsymbol{x}} + \eta_{\boldsymbol{x}} \tag{38}$$

5. Case studies

The performance of this technique was tested on the IEEE 33-node radial system [52,53] (Fig. 2) by using MATLAB. The computer used in this study had a processor Intel (R) Pentium (R) Dual CPU, 1.60 GHz, 2 GB RAM. Table 1 shows the load data in the test system, modelled as normal variables.

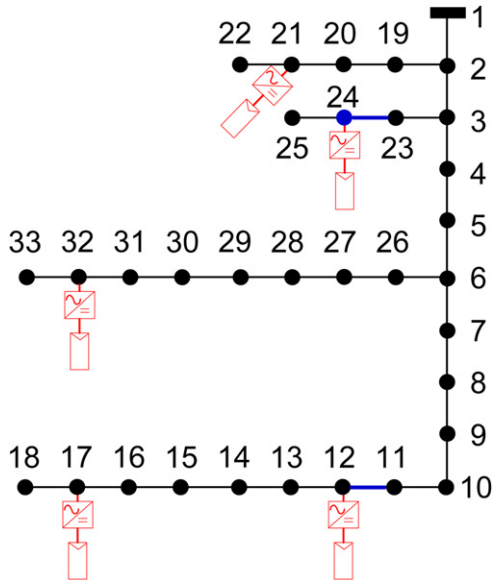

Fig. 2. IEEE 33-node radial system [52,53].

Table 1
Node loads for the IEEE 33-bus radial system for a summer working day at 12:00 a.m.

Node, k	Type	Real power		Reactive power	
		$\eta_{P_{Lk}}$ (pu)	$\sigma_{P_{Lk}}$	$\eta_{Q_{Lk}}$ (pu)	$\sigma_{Q_{Lk}}$
1	Slack	0	0	0	0
2	PQ	0.0010	0.05	0.0006	0.04
3	PQ	0.0009	0.06	0.0004	0.06
4	PQ	0.0012	0.06	0.0008	0.06
5	PQ	0.0006	0.06	0.0003	0.06
6	PQ	0.0006	0.06	0.0002	0.06
7	PQ	0.0020	0.06	0.0010	0.06
8	PQ	0.0020	0.05	0.0010	0.04
9	PQ	0.0006	0.07	0.0002	0.04
10	PQ	0.0006	0.10	0.0002	0.10
11	PQ	0.00045	0.09	0.0003	0.09
12	PQ	0.0006	0.07	0.00035	0.08
13	PQ	0.0006	0.05	0.00035	0.07
14	PQ	0.0012	0.09	0.0008	0.09
15	PQ	0.0006	0.06	0.0001	0.06
16	PQ	0.0006	0.11	0.0002	0.09
17	PQ	0.0006	0.08	0.0002	0.045
18	PQ	0.0009	0.06	0.0004	0.06
19	PQ	0.0009	0.06	0.0004	0.06
20	PQ	0.0009	0.05	0.0004	0.04
21	PQ	0.0009	0.07	0.0004	0.04
22	PQ	0.0009	0.10	0.0004	0.10
23	PQ	0.0009	0.06	0.0005	0.06
24	PQ	0.0042	0.07	0.0020	0.08
25	PQ	0.0042	0.06	0.0020	0.06
26	PQ	0.0006	0.09	0.00025	0.09
27	PQ	0.0006	0.10	0.00025	0.10
28	PQ	0.0006	0.11	0.0002	0.09
29	PQ	0.0012	0.08	0.0007	0.045
30	PQ	0.0020	0.06	0.0060	0.06
31	PQ	0.0015	0.06	0.0007	0.06
32	PQ	0.0021	0.06	0.0010	0.06
33	PQ	0.0006	0.07	0.0004	0.04
	Base (MVA)			Base (kV)	
	100			12.66	

In order to demonstrate the accuracy and efficiency of this technique, its results were compared with the analytical technique based on the Gram–Charlier expansion and the Monte Carlo method with 10,000 trials, which was used as a reference. Thus, Fig. 3 shows the results of error, Eq. (20), and the computation time of the Monte Carlo method as a function of the number of simulations for the test system without PV-DG. In this figure, the number of test groups n_T of the Monte Carlo method for each number of simulations was 50. As can be observed in Fig. 3, the choice of 10,000 simulations for the Monte Carlo method guaranteed that its relative error was lower than 0.005%. In this way, the level of accuracy required of the reference method was achieved.

The test system was then modified including PV generators in order to improve its voltage profile. Five PV generators of the same size were connected to the system in nodes 12, 17, 21, 24 and 32 (Fig. 2). The injected mean PV power was the 61.79% of the load in the base case. In what follows, the results refer to a working day in summer (July) at 12:00 a.m. Fig. 4 shows the seven first cumulants and the PDF of $\boldsymbol{p}_{pv,h}$. These PV generators were introduced as negative loads [2]. Correlation coefficients between PV generators were obtained heuristically from a nearby group of PV generators in

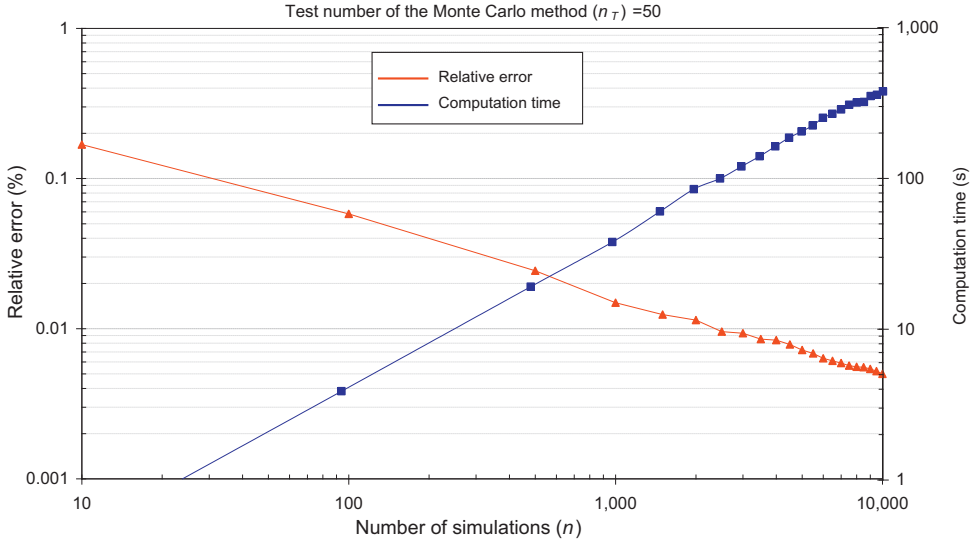

Fig. 3. Relative error and computation time of the Monte Carlo method for the 33-node radial system without PV-GD.

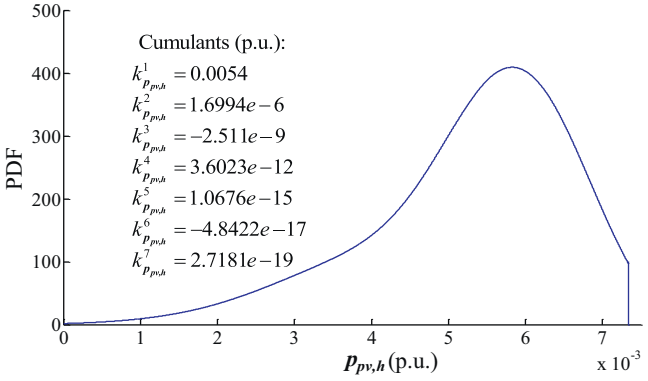

Fig. 4. PDF of the per unit real power for each PV generator on a working day in summer (July) at 12:00 a.m.

Spain. Their values were purposely low, and the correlation matrix was the following:

$$\rho_{pv} = \begin{pmatrix} 1 & 0.15 & 0.18 & 0.16 & 0.13 \\ 0.15 & 1 & 0.25 & 0.22 & 0.14 \\ 0.18 & 0.25 & 1 & 0.17 & 0.23 \\ 0.16 & 0.22 & 0.17 & 1 & 0.19 \\ 0.13 & 0.14 & 0.23 & 0.19 & 1 \end{pmatrix} \quad (39)$$

In order to verify the accuracy of the analytical technique proposed, this technique and the Monte Carlo method were first used to obtain the results for the test system with PV-DG. Table 2 shows the values of individual (average) relative error of the first seven central moments of all the PQ-node voltages in the system. This individual (average) relative error of the *r*-order central moment of the analytical technique $\varepsilon_{\mu^r_{\mathbf{V}_i}}$ ($\varepsilon_{\mu^r_{\mathbf{V}}}$) was defined as [18]:

$$\varepsilon_{\mu^r_{\mathbf{V}_i}} = \frac{100 \cdot \left| \mu^{r,\,\mathbf{an}}_{\mathbf{V}_i} - \mu^{r,\,\mathbf{MC}}_{\mathbf{V}_i} \right|}{\mu^{r,\,\mathbf{MC}}_{\mathbf{V}_i}} \qquad \varepsilon_{\mu^r_{\mathbf{V}}} = \frac{\sum_{i=1}^{i=N_n} \varepsilon^r_{\mathbf{V}_i}}{N_n} \quad (40)$$

The values in Table 2 show the high level of accuracy of the proposed technique for the mean and variance. The higher moments however were less accurate. Regarding the individual relative error of the *r*-order central moment for each node voltage, its maximum value at each order *r* obviously occurred in the PV nodes or nearby nodes: order *#1* (node 18), *#2* (node 17), *#3* (node 24), *#4* (node 17), *#5* (node 24), *#6* (node 25), *#7* (node 24).

The next step was to analyse the optimal number of cumulants to reconstruct the CDFs of the output variables (node voltages) by using the Gram–Charlier or Cornish–Fisher expansion on the particular test system used with PV-GD. The error index selected to evaluate the accuracy of the resulting CDFs with a different number of cumulants was the average-root-mean-square error. This error index statistic is a frequently used measure of the differences between values predicted by a model or an estimator and the values actually observed from the system being modelled or estimated.

Table 2
Individual (average) relative error of the first seven central moments of all PQ-node voltages in the test system with PV-DG.

	$\varepsilon_{\mu^1_{\mathbf{V}_i}}$	$\varepsilon_{\mu^2_{\mathbf{V}_i}}$	$\varepsilon_{\mu^3_{\mathbf{V}_i}}$	$\varepsilon_{\mu^4_{\mathbf{V}_i}}$	$\varepsilon_{\mu^5_{\mathbf{V}_i}}$	$\varepsilon_{\mu^6_{\mathbf{V}_i}}$	$\varepsilon_{\mu^7_{\mathbf{V}_i}}$
Individual (average) relative error of the *r*-order central moment $\varepsilon_{\mu^r_{\mathbf{V}_i}}$ ($\varepsilon_{\mu^r_{\mathbf{V}}}$) (%)							
V_2	0.001	2.713	4.257	6.893	8.409	7.463	7.735
V_3	0.006	3.215	7.749	8.692	9.128	6.994	13.499
V_4	0.010	3.634	4.926	10.209	5.738	6.550	9.700
V_5	0.014	3.762	4.113	10.791	4.879	6.337	9.175
V_6	0.024	3.993	3.156	11.636	4.155	6.058	9.002
V_7	0.027	4.320	2.943	12.722	4.720	5.742	10.819
V_8	0.040	4.477	2.826	13.988	6.565	5.204	16.189
V_9	0.048	4.438	3.043	14.081	7.168	5.100	17.253
V_{10}	0.055	4.338	3.226	13.948	7.531	5.088	17.701
V_{11}	0.056	4.312	3.251	13.888	7.560	5.099	17.676
***V*12**	0.058	4.262	3.306	13.772	7.619	5.121	17.636
V_{13}	0.064	4.347	3.201	14.374	7.908	4.906	18.079
V_{14}	0.067	4.369	3.196	14.604	8.049	4.823	18.287
V_{15}	0.069	4.370	3.225	14.796	8.199	4.748	18.462
V_{16}	0.071	4.353	3.285	14.993	8.403	4.667	18.734
***V*17**	0.076	**4.497**	3.416	**15.264**	8.729	4.545	19.120
V_{18}	**0.076**	4.306	3.416	15.268	8.722	4.545	19.095
V_{19}	0.001	1.477	4.975	4.775	5.379	7.802	8.018
V_{20}	0.002	0.494	23.261	4.867	8.145	7.558	2.267
***V*21**	0.002	0.461	25.419	4.820	8.659	7.564	2.417
V_{22}	0.002	0.460	23.793	4.784	8.252	7.579	2.138
V_{23}	0.007	2.358	19.212	6.483	19.932	7.498	29.343
***V*24**	0.007	1.418	**45.266**	5.128	**29.733**	7.701	**41.201**
V_{25}	0.007	1.354	33.600	4.793	24.435	**7.810**	34.936
V_{26}	0.025	3.889	3.365	11.320	3.898	6.145	8.011
V_{27}	0.025	3.744	3.719	10.932	3.647	6.247	6.829
V_{28}	0.028	3.295	4.779	10.003	3.070	6.484	3.866
V_{29}	0.030	3.024	5.427	9.630	3.129	6.564	2.975
V_{30}	0.032	2.878	6.019	9.476	3.383	6.586	2.785
V_{31}	0.034	2.665	7.322	9.393	4.188	6.558	3.031
***V*32**	0.034	2.603	7.708	9.363	4.436	6.552	3.126
V_{33}	0.034	2.604	7.696	9.364	4.432	6.552	3.128
	$\varepsilon_{\mu^1_{\mathbf{V}}}$	$\varepsilon_{\mu^2_{\mathbf{V}}}$	$\varepsilon_{\mu^3_{\mathbf{V}}}$	$\varepsilon_{\mu^4_{\mathbf{V}}}$	$\varepsilon_{\mu^5_{\mathbf{V}}}$	$\varepsilon_{\mu^6_{\mathbf{V}}}$	$\varepsilon_{\mu^7_{\mathbf{V}}}$
	0.032	3.196	8.878	10.470	8.069	6.194	12.882

Remarks: the maximum value for each order *r* is shown in bold number; nodes with PV generators are shown in bold letters.

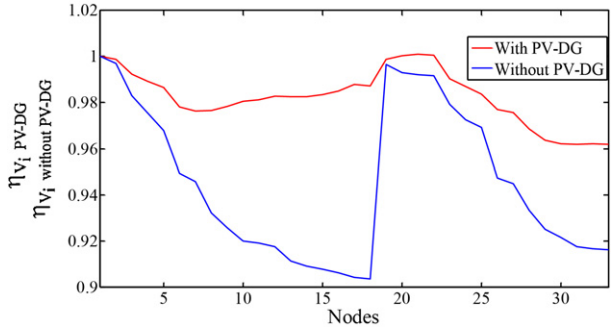

Fig. 5. Mean value of voltage at each feeder node with (without) PV-DG, $\eta_{\mathbf{V}_i \text{ PV-DG}}$ ($\eta_{\mathbf{V}_i \text{ without PV-DG}}$).

The error index statistics for the Gram–Charlier expansion (ε_{GC}) and Cornish–Fisher expansion (ε_{CF}) were defined as [21,22,54]:

$$\varepsilon_{GC} = \frac{\sqrt{\sum_{i=1}^{N_x}(GC_i - MC_i)^2/MC_i^2}}{N_x}100 \quad (41)$$

$$\varepsilon_{CF} = \frac{\sqrt{\sum_{i=1}^{N_x}(GF_i - MC_i)^2/MC_i^2}}{N_x}100 \quad (42)$$

where $GC_i(CF_i)$ and MC_i are the value of the ith point on the CDF using the Gram–Charlier (Cornish–Fisher) expansion and the Monte Carlo method, respectively; and N_x is the number of points considered in x-axis of CDF.

Table 3 shows the maximum Gram–Charlier (Cornish–Fisher) error of all node voltages when 3, 5, 7 and 9 cumulants were used in relevant expansions. It can be seen that the more cumulants were used, the greater the accuracy was. However, as the computation time increased with the number of cumulants, a good level of accuracy with an acceptable computation time was achieved when 7 cumulants were used in the Gram–Charlier expansion and 5 cumulants in the Cornish–Fisher expansion. Computation times in both cases were equivalent, though shorter than the 378.62 s required in the Monte Carlo method.

PV support on critical operating variables of a feeder (e.g. losses, braches load level, nodes voltage profile, etc.) is decisive as shown in [2,45]. In the test system, the allocation of PV generators (Fig. 2) and their penetration level were optimised in order to achieve an improvement of node voltages. Thus, Fig. 5 shows the mean value of voltage at each feeder node with (without) PV-DG, i.e. $\eta_{\mathbf{V}_i \text{ PV-DG}}$ ($\eta_{\mathbf{V}_i \text{ without PV-DG}}$). The connection of PV-DG originated a mean voltage rise in most of nodes. The new voltage profile in nodes was smoother and all voltages remained in their standard limits [55].

The last objective of the case studies was to show the accuracy of the Cornish–Fisher and Gram–Charlier expansions. Thus, the CDFs of apparent powers in lines 23–24 and 12–11 (those with the highest variations) with PV-DG are shown in Fig. 6. Additionally, the CDF of node voltage 24 (the one with the highest variation) is shown in Fig. 7. This last figure shows that at extreme voltage values, the Gram–Charlier expansion gave a bad approximation, whereas the Cornish–Fisher expansion fits better. This behaviour was also observed in CDFs of apparent powers, though the Cornish–Fisher expansion fitting was slightly lower. This was due to the higher non-linearity of reactive power with respect to PV power injection. Both figures show how the proposed technique (Cumulants & Cornish–Fisher expansion) worked better than the technique of the Cumulants & Gram–Charlier expansion, when non-Gaussian functions were involved.

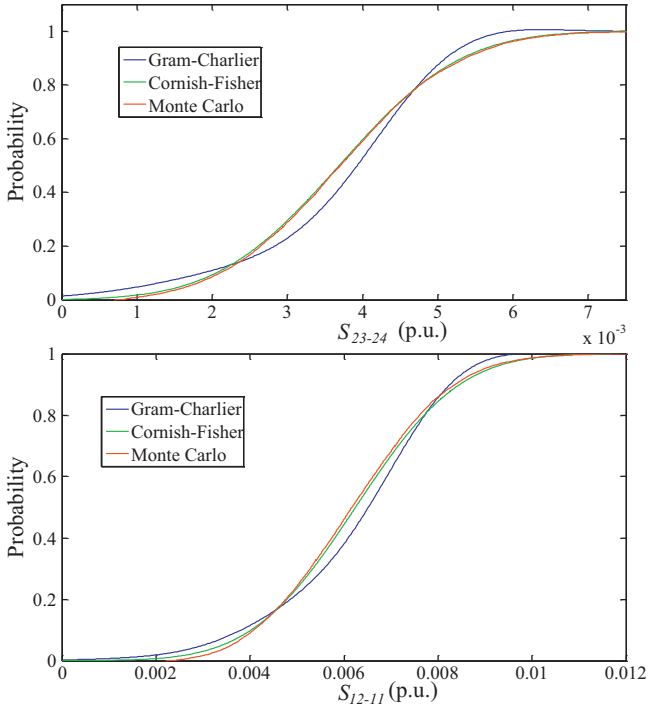

Fig. 6. CDFs of apparent powers in lines 23–24 and 12–11.

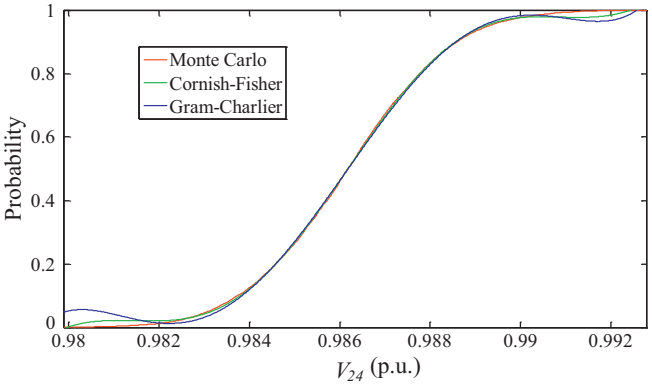

Fig. 7. CDF of node voltage 24.

Table 3
Maximum Gram–Charlier and Cornish–Fisher error in the reconstruction of the CDFs of all node voltages and associated computation time.

	Gram–Charlier expansion		Cornish–Fisher expansion	
	Maximum ε_{GF} of node voltages (%)	Computation time (s)	Maximum ε_{CF} of node voltages (%)	Computation time (s)
3 cumulants	0.389	0.218	0.234	0.195
5 cumulants	0.098	0.301	0.025	0.238
7 cumulants	0.033	0.388	0.021	0.315
9 cumulants	0.031	0.437	0.019	0.398

6. Conclusions

This paper has described a study of voltage profile in radial distribution networks from a stochastic perspective. The probabilistic load flow based on analytical techniques and the Monte Carlo method was used to analyse the impact of the PV-DG.

The analytical method that combined the cumulant method with the Cornish–Fisher expansion was found to be more effective for the evaluation of the impact of the PV-DG on the voltage profiles in distribution networks. This technique gave a better performance than the Monte Carlo method, and provided satisfactory solutions with a smaller number of iterations. Therefore, convergence was rapidly attained and the computational cost was lower than that required for the Monte Carlo method. In addition, the results showed how the Cornish–Fisher expansion had a better performance that the Gram–Charlier expansion, when input random variables were non-Gaussian.

Appendix A.

List of symbols

A PV generator surface area, m^2

B_{ik} series susceptance of branch of node i to node k, pu

CDF cumulative distribution function

$cn_{j,k}$ consumer number who belong to the jth consumer class for the kth node of a feeder

CF_i value of the ith point on the CDF using the Cornish–Fisher expansion

DG distributed generation

$f_{\boldsymbol{p_{pv,h}}}(\boldsymbol{p_{pv,h}})$ and $F_{p_{pv,h}}(\boldsymbol{p_{pv,h}})$ PDF and CDF of random variable $\boldsymbol{p_{pv,h}}$

$FT_b(\theta_s)$ angular loss of radiation beam component, pu

$FT_d(\beta)$, $FT_r(\beta)$ angular losses of each radiation component (d: diffuse, r: ground-reflected), pu

$G_{g,h}$, $G_{b,h}$, $G_{d,h}$, $G_{r,h}$ hourly global, beam, diffuse and ground-reflected (respectively) time-averaged irradiance on horizontal plane, W/m^2

G_{g,h_β} ($H_{g,h}$, $H_{d,h}$) time averaged hourly global irradiance on a surface sloped at angle β to the horizontal, having hourly global irradiation $H_{g,h}$, and hourly diffuse irradiation $H_{d,h}$, W/m^2

G_{ik} series conductance of branch node i to node k, pu

GC_i value of the ith point on the CDF using the Gram–Charlier expansion

h hour of day, h

$H_{0,d}$, $H_{g,d}$ daily extraterrestrial and global (respectively) irradiation on horizontal plane, $MJ \times m^{-2} \times day^{-1}$

$H_{0,h}$, $H_{g,h}$, $H_{d,h}$, $H_{r,h}$ hourly extraterrestrial, global, diffuse and ground-reflected (respectively) irradiation on horizontal plane, $MJ \times m^{-2} \times h^{-1}$

$H_k(x)$ Hermite's polynomial of order k

$\bar{k}_b$ hourly average anisotropy index ($=H_{b,h}/H_{0,h}$), pu

k_t hourly clearness index ($=H_{g,h}/H_{0,h}$), pu

k_d hourly diffuse fraction, pu

k_{dl} lower limit of hourly diffuse fraction, pu

$\bar{k}_d(k_t)$ expected value of hourly diffuse fraction for an event having clearness index k_t, pu

k_x^r cumulant of order r of the univariate random variable $\boldsymbol{x}$

$k_{\boldsymbol{X}}^{\overbrace{i_1 \ldots i_r}^{r}}$ cumulant of order r of the multivariate random variable $\boldsymbol{X}$

K_T daily clearness index, pu

K_{Tu} upper limit of daily clearness index, pu

$\bar{K}_T$ monthly average daily clearness index, pu

$L_j(m,h)$ TDP of the hourly active load for the jth consumer class at mth month and hth hour, W

m month of the year

m_{rv} sample size for a random variable

MC_i value of the ith point on the CDF using the Monte Carlo method

n number of simulations

n_{rv} number of random variables

n_{cc} number of consumer classes

n_T test number of the Monte Carlo method for each number given of simulations

N_n number of nodes of the system

N_x number of points in x-axis of CDF

NOCT normal operating cell temperature, °C

PV photovoltaic

PDF probability density function

$(p_{pv,h})$ $P_{pv,h}$ (per unit) hourly DC input power to a PV inverter, (pu) W

$p_k(\boldsymbol{k_d}, \bar{k}_d)$ PDF of random variable hourly diffuse fraction $\boldsymbol{k_d}$ for a set of hourly events having mean diffuse fraction $\bar{k}_d$

$p_K(\boldsymbol{K_T}, \bar{K}_T)$ PDF of random variable daily clearness index $\boldsymbol{K_T}$ for a set of daily events having mean clearness index $\bar{K}_T$

$P\{Q\}_{Lk}(m,h)$ hourly active {reactive} power consumed by the kth node of a feeder at mth month and hth hour, W{var}

P_i real power injection at node i, pu

Q_i reactive power injection at node i, pu

r_g ratio of the hourly average to the daily average of the global irradiation on a horizontal plane, pu

R_b ratio of beam radiation on the tilted surface to that on a horizontal surface at any time, pu

S_{i-j} apparent power flow between node i and j, pu

TDPs typical daily profiles

T temperature, °C, K

v_w wind speed, m/s

V_i voltage at node i, pu, V

$\bar{V}_i^j$ mean voltage at node ith for the test group jth, given a number of simulations n, pu

x_i value of the of the random variable $\boldsymbol{x}$ in each simulation

Greek symbols

β inclination of the module, °; temperature coefficient, K^{-1}

δ_{ik} phase angle of voltage from node i to node k, pu

ε_{CF} Cornish–Fisher error index statistic, %

ε_{GC} Gram–Charlier error index statistic, %

ε_{MC} relative error of the Monte Carlo method, %

$\varepsilon_{\mu^r_{\boldsymbol{V}_i}}$ individual relative error of the r-order central moment of the node voltage i using the analytical technique, %

ξ PV cell's electrical efficiency, pu

$\eta_{\boldsymbol{x}}$ mean of the random variable $\mathbf{x}$

$\eta_j(m,h)$ hourly mean value of active load for the jth consumer class at mth month and hth hour, W

θ_s irradiance angle of incidence on the tilted surface, °

$\theta(t)$ function relating the hourly mean clearness index to the daily mean clearness index, pu

$\mu^r_{\boldsymbol{x}}$ r-order central moment of the univariate random variable $\boldsymbol{x}$

$\mu_{\boldsymbol{X}}^{\overbrace{i_1 \ldots i_r}^{r}}$ r-order central moment of the multivariate random variable $\boldsymbol{X}$

$\mu^{r,\mathbf{an}}_{\boldsymbol{V}_i}$ r-order central moment of node voltage i found analytically

$\mu^{r,\mathbf{MC}}_{\boldsymbol{V}_i}$ r-order central moment of node voltage i obtained by the Monte Carlo method reflectance of the ground, pu

ρ_{pv} correlation matrix between PV generators

$\sigma_{\boldsymbol{x}}$ standard deviation of the random variable $\boldsymbol{x}$
$\sigma_j(m, h)$ hourly standard deviation of active load for the jth consumer class at mth month and hth hour, W
$\Phi(\boldsymbol{x})$ and $\phi(\boldsymbol{x})$ CDF and PDF, respectively, of a normal $N(0,1)$ distribution ($\eta_{\boldsymbol{x}} = 0, \sigma_{\boldsymbol{x}} = 1$), and $\Phi'(\boldsymbol{x}), \phi'(\boldsymbol{x}), \Phi''(\boldsymbol{x}), \phi''(\boldsymbol{x})\ldots$ their successive derivatives
$\Phi_{\boldsymbol{x}}^{-1}(q)$ q-quantile of a random variable $\boldsymbol{x}$
$\Phi^{-1}(q)$ q-quantile of a standard normal random variable
φ phase angle between the current and voltage, pu

Subscripts
a ambient
c cell/module/generator
NOCT at NOCT conditions
ref at reference conditions

Superscripts
– average value
we weekend days
wo working days

References

[1] F. Jurado, A. Cano, Optimal placement of biomass fuelled gas turbines for reduced losses, Energy Conversion and Management 47 (16) (2006) 2673–2681.
[2] J.C. Hernández, A. Medina, F. Jurado, Optimal allocation and sizing for profitability and voltage enhancement of PV systems on feeders, Renewable Energy 32 (10) (2007) 1768–1789.
[3] R.Y. Rubinstein, Simulation and the Monte Carlo Method, John Wiley and Sons, New York, 1981.
[4] B. Borkowska, Probabilistic load flow, IEEE Transactions on Power Apparatus and Systems 93 (3) (1974) 752–759.
[5] R.N. Allan, B. Borkowska, C.H. Grigg, Probabilistic analysis of power flows, Proceedings of the Institution of Electrical Engineers 121 (12) (1974) 1551–1555.
[6] R.N. Allan, A.M. Leite da Silva, Probabilistic load flow using multilinearisations, IEE Proceedings of Generation, Transmission and Distribution 128 (1981) 280–287.
[7] A.M. Leite da Silva, R.N. Allan, S.M. Soares, V.L. Arienti, Probabilistic load flow considering network outages, IEE Proceedings of Generation, Transmission and Distribution 132 (3) (1985) 139–145.
[8] A.P.S. Meliopoulos, G.J. Cokkinides, X. Yong Chao, A new probabilistic power flow analysis method, IEEE Transactions on Power Systems 5 (1) (1990) 182–190.
[9] P. Zhang, S.T. Lee, Probabilistic load flow computation using the method of combined cumulants and Gram–Charlier expansion, IEEE Transactions on Power Systems 19 (1) (2004) 676–682.
[10] G.J. Anders, Probability Concepts in Electric Power Systems, John Wiley and Sons, New York, 1990.
[11] I.A. Sanabria, T.S. Dillon, Stochastic power flow using cumulants and Von Mises functions, International Journal of Electrical Power and Energy Systems 8 (1) (1986) 47–60.
[12] H. Zhang, P. Li, Probabilistic analysis for optimal power flow under uncertainty, IET Generation, Transmission and Distribution 4 (5) (2010) 553–561.
[13] A. Schellenberg, W. Rosehart, J.A. Aguado, Cumulant-based probabilistic optimal power flow (P-OPF) with Gaussian and gamma distributions, IEEE Transactions on Power Systems 20 (2) (2005) 773–781.
[14] J.M. Morales, J. Pérez-Ruiz, Point estimate schemes to solve the probabilistic power flow, IEEE Transactions on Power Systems 22 (4) (2007) 1594–1601.
[15] P. Caramia, G. Carpinelli, P. Varilone, Point estimate schemes for probabilistic three-phase load flow, Electric Power Systems Research 80 (2) (2010) 168–175.
[16] J. Usaola, Probabilistic load flow with wind production uncertainty using cumulants and Cornish–Fisher expansion, International Journal of Electrical Power and Energy Systems 31 (9) (2009) 474–481.
[17] J. Usaola, Probabilistic load flow in systems with wind generation, IET Generation, Transmission and Distribution 3 (12) (2009) 1031–1041.
[18] J. Usaola, Probabilistic load flow with correlated wind power injections, Electric Power Systems Research 80 (5) (2010) 528–536.
[19] Y.M. Atwa, E.F. El-Saadany, M.M.A. Salama, R. Seethapathy, Optimal renewable resources mix for distribution system energy loss minimization, IEEE Transactions on Power Systems 25 (1) (2010) 360–370.
[20] G. Tina, S. Gagliano, S. Raiti, Hybrid solar/wind power system probabilistic modelling for long-term performance assessment, Solar Energy 80 (5) (2006) 578–588.
[21] S. Yao, Y. Wang, M. Hang, X. Liu, Research on probabilistic power flow of the distribution system with photovoltaic system generation, in: International Conference on Power System Technology (POWERCON), China, 24–28 October, 2010.
[22] R.-x. Fan, S.-n. Wu, Y. Wang, M.-x. Han, The analysis of distribution system with photovoltaic system generation based on probabilistic power flow, in: Asia-Pacific Power and Energy Engineering Conference (APPEEC), China, 25–28 March, 2011.
[23] D. Shirmohammadi, H.W. Hong, A. Semlyen, G.X. Luo, A compensation-based power flow method for weakly Meshed distribution and transmission network, IEEE Transactions on Power Systems 3 (2) (1988) 753–762.
[24] K.G.T. Hollands, R.G. Huget, A probability density function for the clearness index, with applications, Solar Energy 30 (3) (1983) 195–209.
[25] K.G.T. Hollands, S.J. Crha, A probability density function for the diffuse fraction, with applications, Solar Energy 38 (4) (1987) 237–245.
[26] A. Whillier, Solar Energy Collection and its Utilization for House Heating, Ph.D. Thesis in Mechanical Engineering, M.I.T, Cambridge, MA, 1953.
[27] B.Y.H. Liu, R.C. Jordan, The interrelationship and characteristic distribution of direct, diffuse and total solar radiation, Solar Energy 4 (1960) 1–19.
[28] P. Bendt, M. Collares-Pereira, A. Rabl, The frequency distribution of daily isolation values, Solar Energy 27 (1981) 1–5.
[29] G.Y. Saunier, T.A. Reddy, S. Kumar, A monthly probability distribution function of daily global irradiation values appropriate for both tropical and temperate locations, Solar Energy 38 (3) (1987) 169–177.
[30] C. Tiba, A.N. Siqueira, N. Fraidenraich, Cumulative distribution curves of daily clearness index in southern tropical climate, Renewable Energy 32 (2007) 2161–2172.
[31] F. Orgill, K.G.T. Hollands, Correlation equation for hourly diffuse radiation on a horizontal surface, Solar Energy 19 (1977) 357–359.
[32] D.G. Erbs, S.A. Klein, J.A. Duffie, Estimation of the diffuse radiation fraction of hourly, daily, monthly-average global radiation, Solar Energy 28 (1982) 293–302.
[33] D.T. Reindl, W.A. Beckman, J.A. Duffie, Diffuse fraction corrections, Solar Energy 45 (1990) 1–7.
[34] M. Coillares-Pereira, A. Rabl, The average distribution of solar radiation – correlations between diffuse and hemispherical radiation and between daily and hourly insulation values, Solar Energy 22 (2) (1979) 155–164.
[35] A. Luque, S. Hegedus, Handbook of Photovoltaic Science and Engineering, 1st ed., Wiley, Chichester, 2003.
[36] J.E. Hay, D.C. McKay, Estimating solar irradiance on inclined surfaces: a review and assessment of methodologies, International Journal of Sustainable Energy 3 (4&5) (1985) 203–240.
[37] A. Papoulis, S. Pillai, Probability, Random Variables, and Stochastic Processes, 4th ed., McGraw-Hill, New York, 2002.
[38] E. Skoplaki, J.A. Palyvos, On the temperature dependence of photovoltaic module electrical performance: a review of efficiency/power correlations, Solar Energy 83 (2009) 614–624.
[39] C.A. Glasbey, R. Graham, A.G.M. Hunter, Spatio-temporal variability of solar energy across a region: a statistical modelling approach, Solar Energy 70 (4) (2001) 373–438.
[40] B. Kloeckl, G. Papaefthymiou, Multivariate time series models for studies on stochastic generators in power systems, Electric Power Systems Research 80 (3) (2010) 265–276.
[41] K. Ju-Young, J. Gyu-Yeob, H. Won-Hwa, The performance and economical analysis of grid-connected photovoltaic systems in Daegu, Korea, Applied Energy 86 (2) (2009) 265–272.
[42] H.V. Haghi, M.T. Bina, M.A. Golkar, et al., Using Copulas for analysis of large datasets in renewable distributed generation: PV and wind power integration in Iran, Renewable Energy 35 (9) (2010) 1991–2000.
[43] J.A. Jardini, C.M.V. Tahan, M.R. Gouvea, S.U. Ahn, F.M. Figueiredo, Daily load profiles for residential, commercial industrial low voltage consumers, IEEE Transactions on Power Delivery 15 (2000) 375–380.
[44] M. Espinoza, C.J.R. Belmans, B.D. Moor, Short-term load forecasting, profile identification, and customer segmentation: a methodology based on periodic time series, IEEE Transactions on Power Systems 20 (3) (2005) 1622–1630.
[45] J.C. Hernandez, A. Medina, F. Jurado, Impact comparison of PV system integration into rural and urban, Energy Conversion and Management 49 (6) (2008) 1747–1765.
[46] R.N. Allan, A.M. Leite da Silva, R.C. Burchett, Evaluation methods and accuracy in probabilistic load flow solutions, IEEE Transactions on Power Apparatus and Systems 100 (5) (1981) 43–44.
[47] G.C. Canavos, Probabilidad y Estadística. Aplicaciones y Métodos, McGraw-Hill, Virginia, 1988.
[48] M.G. Kendall, A. Stuart, The Advanced Theory of Statistics, Vol. 1., Distribution Theory, Charles Grin and Company Limited, London, 1963.
[49] P. McCullagh, Tensor Methods in Statistics, Chapman and Hall, London, 1987.
[50] I.A. Sanabria, T.S. Dillon, Power system reliability assessment suitable for a deregulated system via the method of cumulants, International Journal of Electrical Power and Energy Systems 20 (3) (1998) 203–211.
[51] E.A. Cornish, R.A. Fisher, Moments and cumulants in the specification of distributions, Revue de l'Institut International de Statis 4 (1937) 307–320.
[52] M.E. Baran, F.F. Wu, Network reconfiguration in distribution systems for loss reduction and load balancing, IEEE Transactions on Power Delivery 4 (2) (1989) 1401–1407.
[53] B. Venkatesh, R. Ranjan, Optimal radial distribution system reconfiguration using fuzzy adaptation of evolutionary programming, International Journal of Electrical Power and Energy Systems 25 (10) (2003) 775–780.
[54] Armstrong, J. Scott, Error measures for generalizing about forecasting methods: empirical comparisons, International Journal of Forecasting 8 (1) (1992) 69–80.
[55] EN 50160, Voltage Characteristics of Electricity Supplied by Public Distribution Systems, 1999.